OPEN ACCESS

Kashf Journal of Multidisciplinary Research
Vol: 03 - Issue 03 (2026)
P-ISSN: 3007-1992 E-ISSN: 3007-200X
https://kjmr.com.pk

DIFFRACTION OF ELECTROMAGNETIC WAVES BY A PARALLEL PLATE WAVEGUIDE WITH IMPEDANCE BOUNDARIES

Ghulam Yameen Mallah[1], Munwar Ayaz Memon[2], Muzaffar Bashir Arain[3], Mehboob Ali Jatoi[4], Darshan Solanki[5]

[1, 4, 5]Department of Basic Science and Related Studies, Quaid-e-Awam University of Engineering, Science and Technology, 67480 Nawabshah, Sindh, Pakistan.

[2]Department of Electrical Engineering, Quaid-e-Awam University of Engineering, Science and Technology, 67480 Nawabshah, Sindh, Pakistan.

[3]Department of Mathematics and Statistics, Quaid-e-Awam University of Engineering, Science and Technology, 67480 Nawabshah, Sindh, Pakistan.

[*]***Corresponding Author:*** (gh.yameen@quest.edu.pk)

DOI:(*https://doi.org/10.71146/kjmr870*)

Article Info

Abstract

This paper presents an analysis of plane wave diffraction by a parallel-plate waveguide structure with mixed boundary conditions. The configuration consists of a perfectly conducting half-plane located at $y = b$ for $x < 0$, and an impedance plane at $y = 0$ with piecewise constant surface impedances $\eta_1$for $x < 0$ and η_2 for $x > 0$. An E-polarized plane wave is considered as the incident field. A mode matching formulation is developed to model the electromagnetic field distribution within the structure. The fields in each region are expanded in terms of waveguide eigen modes, and the continuity conditions at the junction $x = 0$ are enforced to obtain an infinite system of linear algebraic equations. This system is solved numerically using a suitable truncation scheme. The far-field diffracted field is evaluated using the stationary phase method. Numerical results are presented to investigate the influence of waveguide spacing, surface impedance variation, and angle of incidence on the diffraction characteristics. The proposed approach provides an accurate and computationally efficient framework for analyzing diffraction in such waveguide configurations.

Keywords:
Diffraction, parallel plate waveguide, mode matching, impedance boundary conditions, electromagnetic scattering.

1. INTRODUCTION

The diffraction of electromagnetic waves by waveguide structures has been a long-standing problem in applied electromagnetics due to its importance in both theoretical analysis and practical applications. Parallel-plate waveguides serve as fundamental canonical models widely used in microwave engineering, optical systems, and antenna design. When a plane wave is incident on the open end of such a waveguide, complex scattering phenomena occur, leading to the excitation of guided modes inside the structure and radiated fields in the surrounding space. The analytical treatment of such diffraction problems involving semi-infinite geometries has traditionally been based on the Wiener–Hopf technique [1], which provides a rigorous mathematical framework for solving boundary value problems in open structures. This method has been extensively developed in classical literature and remains a cornerstone of diffraction theory. Extensions to waveguide problems have been reported in the literature. In particular, Matrix Wiener–Hopf formulations was developed for impedance-loaded parallel-plate waveguides, reducing the problem to coupled infinite systems of algebraic equations in [2] and [10]. However, the method involves kernel factorization, which becomes highly complex in matrix cases and limits its practical applicability [11]. The mode matching method provides an effective alternative for analyzing waveguide scattering problems. This technique expands the electromagnetic fields in terms of waveguide eigenmodes and enforces continuity conditions at interfaces. As a result, the problem is transformed into a system of linear algebraic equations that can be solved numerically in a straightforward manner. The method has been widely used for waveguide discontinuities and scattering problems and is known for its computational efficiency and simplicity [3,4,14]. The inclusion of impedance boundary conditions significantly improves the physical realism of the model. Impedance surfaces are widely used to represent lossy dielectric coatings, absorbing materials, and engineered metamaterial surfaces [15–17]. In modern electromagnetic engineering, such surfaces are also employed for wave manipulation and antenna performance enhancement. Discontinuities in surface impedance introduce additional scattering complexity and give rise to rich diffraction phenomena in waveguide configurations. Recent developments have further extended its application to complex impedance structures and discontinuous boundaries [19], as well as structured waveguide configurations studied using modern computational approaches [20,21]. These studies demonstrate the growing importance of mode matching in contemporary electromagnetic analysis.

In the present work, the mode matching method is applied to the diffraction of a plane wave by a parallel-plate waveguide with a two-part impedance boundary. The formulation avoids analytical kernel factorization and provides a simple and efficient computational framework. Moreover, the approach is flexible and can be extended to more general impedance distributions and geometrical configurations, making it suitable for a wide class of electromagnetic scattering problems.

The remainder of this paper is organized as follows. Section 2 presents the mathematical formulation of the problem. Section 3 describes the mode matching solution procedure. Section 4 discusses the far-field evaluation and Section 5 includes the numerical results and discussion. Finally, Section 5 concludes the paper.

2. MATHEMATICAL FORMULATION OF THE PROBLEM

Consider a structure of two-dimensional waveguide consists of a perfectly conducting half-plane occupying the region $y = b$ for $x < 0$, while the lower boundary at $y = 0$ is modelled as an impedance plane. The surface impedance is piecewise constant, taking values η_1 for $x < 0$ and η_2 for $x > 0$, respectively. Since the structure is invariant along the z-direction, the problem reduces to a two-dimensional formulation with all field quantities independent of z.

An E-polarized time-harmonic plane wave is incident from the region $y > b$ at an angle θ_0 measured from the positive x-axis. The incident electric field in z-component is given by

$$v_i(x, y) = e^{-ik(x\cos\theta_0 - y\sin\theta_0)}, \tag{1}$$

where $k = \omega/c = 2\pi/\lambda$ is the free-space wavenumber, and the time factor $e^{-i\omega t}$ is suppressed throughout the analysis. The total field in each region consists of incident, reflected, and scattered components, depending on the geometry.

The total field satisfies the two-dimensional Helmholtz equation in all regions,

$$\frac{\partial^2 v}{\partial x^2} + \frac{\partial^2 v}{\partial y^2} + k^2 v = 0, \tag{2}$$

which follows directly from Maxwell's equations for the z-component of the electric field in a homogeneous, source-free medium [3,4].

The boundary conditions are specified as follows. On the perfectly conducting surface at $y = b$ for $x < 0$, the tangential electric field vanishes, leading to

$$\mathrm{v}(\mathrm{x}, \mathrm{b}) = 0, \mathrm{x} < 0, \tag{3}$$

On the impedance plane at $\mathrm{y} = 0$, the surface impedance boundary condition relates the field to its normal derivative. This gives

$$\left(1 + \frac{\eta_1}{\mathrm{ik}}\frac{\partial}{\partial \mathrm{y}}\right)\mathrm{v}(\mathrm{x}, 0) = 0, \mathrm{x} < 0, \tag{4}$$

$$\left(1 + \frac{\eta_2}{\mathrm{ik}}\frac{\partial}{\partial \mathrm{y}}\right)\mathrm{v}(\mathrm{x}, 0) = 0, \mathrm{x} > 0, \tag{5}$$

These conditions model partially reflecting surfaces and generalize the classical perfect electric conductor (PEC) and perfect magnetic conductor (PMC) cases commonly used in electromagnetic boundary modelling [15,16].

The field representation is divided into three regions. Region I ($y > b$) contains the incident field, the reflected wave from the conducting boundary, and the scattered field radiating to infinity. Region II ($0 < y < b$) represents the parallel-plate waveguide region supporting both propagating and evanescent modes. Region III ($y < 0$) corresponds to the lower half-space governed by the impedance boundary, where fields decay away from the interface.

At the interface $y = b$, continuity of tangential field components is enforced for all x, giving

$$v_1(x, b) = v_2(x, b), -\infty < x < \infty, \tag{6}$$

$$\frac{\partial v_1}{\partial y}(x, b) = \frac{\partial v_2}{\partial y}(x, b), -\infty < x < \infty, \tag{7}$$

The scattered field must satisfy the Sommerfeld radiation condition to ensure outgoing wave behaviour at infinity,

$$\sqrt{\rho}\left(\frac{\partial v_s}{\partial \rho} - ikv_s\right) \to 0, \rho \to \infty, \tag{8}$$

where $\rho = \sqrt{x^2 + y^2}$. This condition ensures uniqueness of the radiating solution [1,2].

Finally, near the edge points at $(0, 0)$ and $(0, b)$, the field must satisfy Meixner's edge conditions to ensure finite energy. The local behavior of the field is given by

$$v = O(r^{1/2}), \frac{\partial v}{\partial n} = O(r^{-1/2}), r \to 0, \tag{9}$$

where rdenotes the distance from the edge. Such conditions are essential in diffraction problems involving sharp discontinuities and are well established in classical electromagnetic theory [6,7].

3. MODE EXPANSIONS FOR MODE MATCHING FORMULATION

The mode matching method begins by expanding the field in each region as a superposition of eigenfunctions (modes) that individually satisfy the Helmholtz equation and the boundary conditions on the horizontal boundaries. The unknown coefficients are determined by enforcing continuity across the vertical line $x = 0$.

In Region II $0 < y < b$, the field is confined between the lower impedance plane at $y = 0$ and the upper conducting plate at $y = b$. The eigenfunctions are obtained by solving the Sturm-Liouville problem:

$$\frac{d^2Y}{dy^2} + \lambda^2 Y = 0, \tag{10}$$

with boundary conditions:

$$Y(b) = 0, \tag{11}$$

and

$$\frac{dY}{dy}(0) + ik\eta_2 Y(0) = 0, \tag{12}$$

Dirichlet at conducting plate and Impedance at $y = 0$ respectively, where η_2 is used for the eigenfunctions because Region II is primarily influenced by the impedance on the right side ($x > 0$) where energy propagates. The effect of the impedance discontinuity will be handled through the matching conditions.

The general solution of (10) is:

$$Y(y) = A\cos(\lambda y) + B\sin(\lambda y), \tag{13}$$

Applying the boundary condition at $y = b$:

$$A\cos(\lambda b) + B\sin(\lambda b) = 0 \Rightarrow B = -A\frac{\cos(\lambda b)}{\sin(\lambda b)}, \tag{14}$$

provided $sin\,(\lambda b) \neq 0$. Substituting into (13):

$$Y(y) = A\left[\cos(\lambda y) - \frac{\cos(\lambda b)}{\sin(\lambda b)}\sin(\lambda y)\right] = \frac{A}{\sin(\lambda b)}[\sin(\lambda b)\cos(\lambda y) - \cos(\lambda b)\sin(\lambda y)], \tag{15}$$

Using the trigonometric identity $sin\,(\lambda b)cos\,(\lambda y) - cos\,(\lambda b)sin\,(\lambda y) = sin\,(\lambda(b - y))$, it can be obtained that:

$$Y(y) = C\sin(\lambda(b - y)), \tag{16}$$

where $C = A/sin\,(\lambda b)$ is a constant.

Now apply the impedance boundary condition at $y = 0$:

$$\frac{dY}{dy}(0) + ik\eta_2 Y(0) = 0, \tag{17}$$

From (16):

$$\frac{dY}{dy} = -C\lambda\cos(\lambda(b - y)), \tag{18}$$

Thus at $y = 0$:

$$\frac{dY}{dy}(0) = -C\lambda\cos(\lambda b), \tag{19}$$

$$Y(0) = C\sin(\lambda b), \tag{20}$$

Substituting into (17):

$$-C\lambda\cos(\lambda b) + ik\eta_2 C\sin(\lambda b) = 0, \tag{21}$$

Dividing by $Ccos\,(\lambda b)$ (assuming $cos\,(\lambda b) \neq 0$):

$$-\lambda + ik\eta_2\tan(\lambda b) = 0, \tag{22}$$

This gives the eigenvalue equation:

$$\tan(\lambda_n b) = \frac{\lambda_n}{ik\eta_2} = -i\frac{\lambda_n}{k\eta_2}, \tag{23}$$

For purely imaginary η_2 (reactive surface), the right-hand side is real. The eigenvalues λ_n are real for propagating modes and imaginary for evanescent modes. The index $n = 0,1,2,\ldots$ enumerates the solutions.

The eigenfunctions are orthonormalized:

$$\phi_n(y) = \sqrt{\frac{2}{b}}\sin(\lambda_n(b-y)), \tag{24}$$

with the orthonormality condition:

$$\int_0^b \phi_n(y)\phi_m(y)dy = \delta_{nm}, \tag{25}$$

where δ_{nm} is the Kronecker delta.

The field in Region II is expanded as a sum of forward and backward traveling waves:

$$v_2(x,y) = \sum_{n=0}^{\infty} A_n e^{i\gamma_n x}\phi_n(y) + \sum_{n=0}^{\infty} B_n e^{-i\gamma_n x}\phi_n(y), \tag{26}$$

where A_n are coefficients for waves traveling in the $+x$ direction (to the right), B_n are coefficients for waves traveling in the $-x$ direction (to the left) and $\gamma_n = \sqrt{k^2 - \lambda_n^2}$ is the propagation constant. For propagating modes, $\lambda_n < k$ and γ_n is real. For evanescent modes, $\lambda_n > k$ and $\gamma_n = i\,|\,\gamma_n\,|$ is imaginary, representing exponentially decaying fields.

In Region I $0 < y > b$, the field consists of the incident plane wave, the wave reflected from the conducting plate, and the scattered field. The incident and reflected waves together satisfy the boundary condition at $y = b$ in the absence of the aperture.

The incident wave from (1) at $y = b$ is:

$$v_i(x,b) = e^{-ikx\cos\theta_0}e^{ikb\sin\theta_0}. \tag{27}$$

The reflected wave from the conducting plate (assuming an infinite plate at $y = b$ for all x) is:

$$v_r(x,y) = -e^{-ikx\cos\theta_0}e^{-ik(y-b)\sin\theta_0}. \tag{28}$$

This satisfies $v_i + v_r = 0$ at $y = b$. The total incident-plus-reflected field is:

$$v_{inc}(x,y) = e^{-ikx\cos\theta_0}\left[e^{ik(y-b)\sin\theta_0} - e^{-ik(y-b)\sin\theta_0}\right] = 2ie^{-ikx\cos\theta_0}\sin(k(y-b)\sin\theta_0). \tag{29}$$

The scattered field is represented as an integral over plane waves (continuous spectrum):

$$v_s(x,y) = \int_{-\infty}^{\infty} S(\alpha)\, e^{i\alpha x}e^{i\sqrt{k^2-\alpha^2}(y-b)}d\alpha, \tag{30}$$

where $S(\alpha)$ is the unknown spectral amplitude. The square root is defined with $Im\ (\sqrt{k^2-\alpha^2}) \geq 0$ to ensure outgoing wave behavior.

Thus, the total field in Region I is:

$$v_1(x,y) = 2ie^{-ikxcos\ \theta_0}sin\ (k(y-b)sin\ \theta_0) + \int_{-\infty}^{\infty} S(\alpha)\, e^{i\alpha x}e^{i\sqrt{k^2-\alpha^2}(y-b)}d\alpha. \quad (31)$$

For numerical implementation, we discretize the continuous spectrum. Let α_n be sampling points. Then:

$$v_1(x,y) \approx 2ie^{-ikxcos\ \theta_0}sin\ (k(y-b)sin\ \theta_0) + \sum_{n=0}^{N-1} C_n\, e^{i\alpha_n x}e^{i\sqrt{k^2-\alpha_n^2}(y-b)}, \quad (32)$$

where $C_n = S(\alpha_n)\Delta\alpha$ with $\Delta\alpha$ the sampling interval.

In Region III ($y < 0$), below the impedance plane, the field must decay as $y \to -\infty$. The appropriate expansion uses modes that satisfy the impedance condition at $y = 0$ and decay exponentially:

$$v_3(x,y) = \sum_{m=0}^{\infty} D_m\, e^{i\xi_m x}e^{\nu_m y}, \quad (33)$$

where $\nu_m = \sqrt{\xi_m^2 - k^2}$ with $Re\ (\nu_m) > 0$ to ensure decay as $y \to -\infty$. The eigenvalues ξ_m are determined by the impedance boundary condition at $y = 0$:

$$\left(1+\frac{\eta_2}{ik}\frac{\partial}{\partial y}\right)v_3(x,0) = 0. \quad (34)$$

Substituting (33) into (34):

$$1+\frac{\eta_2}{ik}\nu_m = 0 \Rightarrow \nu_m = -\frac{ik}{\eta_2}. \quad (35)$$

Thus:

$$\sqrt{\xi_m^2 - k^2} = -\frac{ik}{\eta_2}. \quad (36)$$

Squaring both sides:

$$\xi_m^2 - k^2 = -\frac{k^2}{\eta_2^2}, \quad (37)$$

$$\xi_m^2 = k^2\left(1-\frac{1}{\eta_2^2}\right). \quad (38)$$

Therefore:

$$\xi_m = \pm k\sqrt{1-\frac{1}{\eta_2^2}}. \quad (39)$$

For a passive impedance, $Im\ (\eta_2) > 0$, and the appropriate branch is chosen so that waves propagate away from the aperture or decay.

For simplicity in this analysis, we note that Region III contributes minimally to the diffracted field in the far zone when the impedance is highly reflective. We will focus on Regions I and II, which dominate the scattering.

For Mode Matching Formulation, the unknown coefficients A_n, B_n, and C_n (or $S(\alpha)$) are determined by enforcing continuity of the field and its x-derivative across the vertical line $x = 0$ for $0 < y < b$. This aperture is the interface between Region I (for $x > 0$) and Region II (for $x < 0$).

For $0 < y < b$, the field must be continuous across $x = 0$:

$$v_1(0^+, y) = v_2(0^-, y). \tag{40}$$

The tangential magnetic field (proportional to $\partial v/\partial x$) must also be continuous:

$$\frac{\partial v_1}{\partial x}(0^+, y) = \frac{\partial v_2}{\partial x}(0^-, y). \tag{41}$$

Substituting the expansions from Sections 3.1 and 3.2:

For $x = 0^+$:

$$v_1(0, y) = 2i\sin(k(y - b)\sin\theta_0) + \int_{-\infty}^{\infty} S(\alpha)\, e^{i\sqrt{k^2-\alpha^2}(y-b)} d\alpha, \tag{42}$$

$$\frac{\partial v_1}{\partial x}(0, y) = -2ik\cos\theta_0 \cdot 2i\sin(k(y - b)\sin\theta_0). \tag{43}$$

At $x = 0$:

$$\frac{\partial v_{inc}}{\partial x}(0, y) = 2k\cos\theta_0 \sin(k(y - b)\sin\theta_0). \tag{44}$$

For the scattered part at $x = 0$:

$$\frac{\partial v_s}{\partial x}(0, y) = \int_{-\infty}^{\infty} i\alpha S(\alpha)\, e^{i\sqrt{k^2-\alpha^2}(y-b)} d\alpha. \tag{45}$$

For $x = 0^-$ (Region II):

$$v_2(0, y) = \sum_{n=0}^{\infty} (A_n + B_n)\phi_n(y), \tag{46}$$

$$\frac{\partial v_2}{\partial x}(0, y) = \sum_{n=0}^{\infty} i\gamma_n (A_n - B_n)\phi_n(y). \tag{47}$$

To convert the functional equations (40)-(41) into algebraic equations, we multiply both sides by $\phi_m(y)$ and integrate from $y = 0$ to $y = b$. Using the orthonormality condition (25):

$$\int_0^b \phi_m(y)\phi_n(y) dy = \delta_{mn}. \tag{48}$$

From (40):

$$\int_0^b v_1(0, y)\phi_m(y) dy = \int_0^b \sum_{n=0}^{\infty} (A_n + B_n)\phi_n(y)\phi_m(y) dy = A_m + B_m. \tag{49}$$

Thus:

$$A_m + B_m = \int_0^b \left[2i\sin(k(y-b)\sin\theta_0) + \int_{-\infty}^{\infty} S(\alpha)e^{i\sqrt{k^2-\alpha^2}(y-b)}d\alpha\right]\phi_m(y)dy. \quad (50)$$

From (41):

$$\int_0^b \frac{\partial v_1}{\partial x}(0,y)\phi_m(y)dy = \int_0^b \sum_{n=0}^{\infty} i\gamma_n(A_n - B_n)\phi_n(y)\phi_m(y)dy = i\gamma_m(A_m - B_m). \quad (51)$$

Thus:

$$i\gamma_m(A_m - B_m) = \int_0^b \left[2k\cos\theta_0\sin(k(y-b)\sin\theta_0) + \int_{-\infty}^{\infty} i\alpha S(\alpha)e^{i\sqrt{k^2-\alpha^2}(y-b)}d\alpha\right]\phi_m(y)dy. \quad (52)$$

To Evaluate the known integrals, define the following integrals:

$$F_m = \int_0^b 2i\sin(k(y-b)\sin\theta_0)\phi_m(y)dy, \quad (53)$$

$$G_m = \int_0^b 2k\cos\theta_0\sin(k(y-b)\sin\theta_0)\phi_m(y)dy, \quad (54)$$

$$I_m(\alpha) = \int_0^b e^{i\sqrt{k^2-\alpha^2}(y-b)}\phi_m(y)dy, \quad (55)$$

$$J_m(\alpha) = \int_0^b i\alpha e^{i\sqrt{k^2-\alpha^2}(y-b)}\phi_m(y)dy. \quad (56)$$

These integrals can be evaluated analytically. Substituting $\phi_m(y) = \sqrt{2/b}\sin(\lambda_m(b-y))$:

For F_m:

$$F_m = 2i\sqrt{\frac{2}{b}}\int_0^b \sin(k(y-b)\sin\theta_0)\sin(\lambda_m(b-y))dy. \quad (57)$$

Let $u = b - y$. Then $dy = -du$, and when $y = 0, u = b$; when $y = b, u = 0$. Also $y - b = -u$.

Thus:

$$\sin(k(y-b)\sin\theta_0) = \sin(-k\sin\theta_0) = -\sin(k\sin\theta_0), \quad (58)$$

$$\sin(\lambda_m(b-y)) = \sin(\lambda_m u). \quad (59)$$

Therefore:

$$F_m = 2i\sqrt{\frac{2}{b}}\int_{u=b}^{0}[-\sin(k\sin\theta_0)]\sin(\lambda_m u)(-du) = 2i\sqrt{\frac{2}{b}}\int_0^b \sin(k\sin\theta_0)\sin(\lambda_m u)du. \quad (60)$$

The integral is standard:

$$\int_0^b \sin(pu)\sin(qu)du = \frac{1}{2}\left[\frac{\sin((p-q)b)}{p-q} - \frac{\sin((p+q)b)}{p+q}\right], p \neq \pm q. \quad (61)$$

Thus with $p = k\sin\theta_0$ and $q = \lambda_m$:

$$F_m = 2i\sqrt{\frac{2}{b}} \cdot \frac{1}{2}\left[\frac{\sin((k\sin\theta_0 - \lambda_m)b)}{k\sin\theta_0 - \lambda_m} - \frac{\sin((k\sin\theta_0 + \lambda_m)b)}{k\sin\theta_0 + \lambda_m}\right]. \quad (62)$$

Simplifying:

$$F_m = i\sqrt{\frac{2}{b}}\left[\frac{\sin((k\sin\theta_0 - \lambda_m)b)}{k\sin\theta_0 - \lambda_m} - \frac{\sin((k\sin\theta_0 + \lambda_m)b)}{k\sin\theta_0 + \lambda_m}\right]. \quad (63)$$

For G_m:

$$G_m = 2k\cos\theta_0\sqrt{\frac{2}{b}}\int_0^b \sin(k u\sin\theta_0)\sin(\lambda_m u)du. \quad (64)$$

Using the same integral:

$$G_m = 2k\cos\theta_0\sqrt{\frac{2}{b}} \cdot \frac{1}{2}\left[\frac{\sin((k\sin\theta_0 - \lambda_m)b)}{k\sin\theta_0 - \lambda_m} - \frac{\sin((k\sin\theta_0 + \lambda_m)b)}{k\sin\theta_0 + \lambda_m}\right], \quad (65)$$

$$G_m = k\cos\theta_0\sqrt{\frac{2}{b}}\left[\frac{\sin((k\sin\theta_0 - \lambda_m)b)}{k\sin\theta_0 - \lambda_m} - \frac{\sin((k\sin\theta_0 + \lambda_m)b)}{k\sin\theta_0 + \lambda_m}\right]. \quad (66)$$

For $I_m(\alpha)$:

$$I_m(\alpha) = \sqrt{\frac{2}{b}}\int_0^b e^{i\sqrt{k^2-\alpha^2}(y-b)}\sin(\lambda_m(b-y))dy. \quad (67)$$

Let $u = b - y$ as before. Then $y - b = -u$, and $dy = -du$:

$$I_m(\alpha) = \sqrt{\frac{2}{b}}\int_{u=b}^0 e^{-i\sqrt{k^2-\alpha^2}u}\sin(\lambda_m u)(-du) = \sqrt{\frac{2}{b}}\int_0^b e^{-i\beta u}\sin(\lambda_m u)du, \quad (68)$$

where $\beta = \sqrt{k^2 - \alpha^2}$. The integral is:

$$\int_0^b e^{-i\beta u}\sin(\lambda u)du = \frac{\lambda - e^{-i\beta b}(\lambda\cos(\lambda b) + i\beta\sin(\lambda b))}{\lambda^2 - \beta^2}. \quad (69)$$

Thus:

$$I_m(\alpha) = \sqrt{\frac{2}{b}} \cdot \frac{\lambda_m - e^{-i\beta b}(\lambda_m\cos(\lambda_m b) + i\beta\sin(\lambda_m b))}{\lambda_m^2 - \beta^2}. \quad (70)$$

Note that $\lambda_m^2 - \beta^2 = \lambda_m^2 - (k^2 - \alpha^2) = \lambda_m^2 - k^2 + \alpha^2$.

For $J_m(\alpha)$:

$$J_m(\alpha) = i\alpha I_m(\alpha). \quad (71)$$

For numerical implementation, we discretize the continuous spectrum integrals using a quadrature rule.

Let α_p be quadrature points with weights w_p. Then:

$$\int_{-\infty}^{\infty} S(\alpha)\, I_m(\alpha)d\alpha \approx \sum_{p=0}^{P-1} S(\alpha_p)I_m(\alpha_p)w_p. \quad (72)$$

Define $C_p = S(\alpha_p)w_p$. Then:

$$A_m + B_m = F_m + \sum_{p=0}^{P-1} C_p\, I_m(\alpha_p), \tag{73}$$

$$i\gamma_m(A_m - B_m) = G_m + \sum_{p=0}^{P-1} C_p\, J_m(\alpha_p). \tag{74}$$

These are two equations relating A_m, B_m, and C_p.

A_m and B_m can be solved in terms of C_p from Eq. (73) and (74):

Add (73) and (74)/$i\gamma_m$:

$$2A_m = F_m + \frac{G_m}{i\gamma_m} + \sum_{p=0}^{P-1} C_p \left[I_m(\alpha_p) + \frac{J_m(\alpha_p)}{i\gamma_m}\right]. \tag{75}$$

Thus:

$$A_m = \frac{1}{2}\left[F_m + \frac{G_m}{i\gamma_m}\right] + \frac{1}{2}\sum_{p=0}^{P-1} C_p \left[I_m(\alpha_p) + \frac{J_m(\alpha_p)}{i\gamma_m}\right]. \tag{76}$$

Subtract (73) from (74)/$i\gamma_m$:

$$-2B_m = -F_m + \frac{G_m}{i\gamma_m} + \sum_{p=0}^{P-1} C_p \left[-I_m(\alpha_p) + \frac{J_m(\alpha_p)}{i\gamma_m}\right]. \tag{77}$$

Thus:

$$B_m = \frac{1}{2}\left[F_m - \frac{G_m}{i\gamma_m}\right] + \frac{1}{2}\sum_{p=0}^{P-1} C_p \left[I_m(\alpha_p) - \frac{J_m(\alpha_p)}{i\gamma_m}\right]. \tag{78}$$

For the remaining condition as no incoming waves from the left for $x < 0$ in Region II, the coefficients B_n represent waves traveling to the left (toward the aperture). There should be no waves incident from the left (i.e., from $x = -\infty$) except those generated by scattering. However, the A_n coefficients represent waves traveling to the right (away from the aperture). The condition that no energy comes from $x = -\infty$ is already satisfied by our expansion. The remaining condition is that the field in Region I for $x < 0$ must be consistent with the field in Region II. This gives an additional equation relating the C_p coefficients to themselves.

Alternatively, we can use the condition that the total field on the conducting plate for $x < 0$ is automatically zero because $\phi_n(b) = 0$. No further condition is needed.

The unknown coefficients C_p are determined by requiring that the field representation in Region I (for $x < 0$) matches the field in Region II when extended to $x < 0$. This leads to an integral equation that, after discretization, becomes:

$$\sum_{p=0}^{P-1} C_p \left[\delta_{pq} + K_{pq}\right] = H_q, \tag{79}$$

where K_{pq} and H_q are derived from the mode matching conditions. The explicit form of K_{pq} is:

$$K_{pq} = \sum_{m=0}^{\infty} \frac{1}{2}\left[I_m(\alpha_p) + \frac{J_m(\alpha_p)}{i\gamma_m}\right]\left[I_m(\alpha_q) - \frac{J_m(\alpha_q)}{i\gamma_m}\right], \quad (80)$$

and

$$H_q = -\sum_{m=0}^{\infty} \frac{1}{2}\left[F_m + \frac{G_m}{i\gamma_m}\right]\left[I_m(\alpha_q) - \frac{J_m(\alpha_q)}{i\gamma_m}\right], \quad (81)$$

The infinite sum over m is truncated to M terms. The resulting linear system is solved numerically for the coefficients C_p.

4. FAR FIELD COMPUTATION

Once the coefficients C_p are known, the diffracted field in the far zone can be computed using the method of stationary phase that is also called the steepest descent method.

To find the stationary phase for the scattered field in Region I is given by (30):

$$v_s(\rho,\theta) = \int_{-\infty}^{\infty} S(\alpha)\, e^{i\alpha x} e^{i\sqrt{k^2-\alpha^2}(y-b)} d\alpha, \quad (82)$$

In polar coordinates: $x = \rho cos\ \theta$, $y = \rho sin\ \theta$. For large ρ, the phase function is:

$$\Phi(\alpha) = \alpha\cos\ \theta + \sqrt{k^2-\alpha^2}\sin\ \theta, \quad (83)$$

The stationary point occurs where $\Phi'(\alpha) = 0$:

$$\Phi'(\alpha) = \cos\ \theta - \frac{\alpha}{\sqrt{k^2-\alpha^2}}\sin\ \theta = 0, \quad (84)$$

Solving:

$$\cos\ \theta = \frac{\alpha}{\sqrt{k^2-\alpha^2}}\sin\ \theta \Rightarrow \cot\ \theta = \frac{\alpha}{\sqrt{k^2-\alpha^2}}, \quad (85)$$

Squaring:

$$\cot^2\theta = \frac{\alpha^2}{k^2-\alpha^2}, \quad (86)$$

$$\alpha^2 = k^2\cos^2\theta. \quad (87)$$

Thus:

$$\alpha_0 = -k\cos\ \theta. \quad (88)$$

The negative sign is chosen to satisfy the radiation condition. The second derivative at the stationary point:

$$\Phi''(\alpha) = -\frac{k^2}{(k^2-\alpha^2)^{3/2}}\sin\ \theta. \quad (89)$$

At $\alpha_0 = -k cos\ \theta$:

$$k^2 - \alpha_0^2 = k^2 - k^2\cos^2\theta = k^2\sin^2\theta, \tag{90}$$

$$\sqrt{k^2 - \alpha_0^2} = k\sin\theta, \tag{91}$$

$$\Phi''(\alpha_0) = -\frac{k^2}{(k^2\sin^2\theta)^{3/2}}\sin\theta = -\frac{k^2}{k^3|\sin\theta|^3}\sin\theta = -\frac{1}{k\sin^2\theta}. \tag{92}$$

The stationary phase formula gives:

$$\int_{-\infty}^{\infty} S(\alpha)\, e^{i\rho\Phi(\alpha)} d\alpha \sim S(\alpha_0) e^{i\rho\Phi(\alpha_0)} \sqrt{\frac{2\pi}{\rho|\Phi''(\alpha_0)|}} e^{i\pi/4 \cdot \mathrm{sign}(\Phi''(\alpha_0))}. \tag{93}$$

Since $\Phi''(\alpha_0) < 0$ for $\theta \in (0, \pi)$, the sign is -1, so the phase factor is $e^{-i\pi/4}$.

Now:

$$\Phi(\alpha_0) = \alpha_0\cos\theta + \sqrt{k^2 - \alpha_0^2}\sin\theta = (-k\cos\theta)\cos\theta + (k\sin\theta)\sin\theta = -k\cos^2\theta + k\sin^2\theta. \tag{94}$$

However, a simpler expression is:

$$\Phi(\alpha_0) = k[-\cos^2\theta + \sin^2\theta] = -k\cos(2\theta). \tag{95}$$

But note that $y - b = \rho sin\ \theta - b$. For large ρ, b is negligible, so:

$$v_s(\rho, \theta) \sim S(-k\cos\theta) e^{-ikb\sin\theta} e^{ik\rho} \sqrt{\frac{2\pi}{k\rho}} e^{-i\pi/4}. \tag{96}$$

where we have included the factor $e^{-ikbsin\ \theta}$ from the $y - b$ dependence.

Thus, the far field amplitude is proportional to $|\ S(-kcos\ \theta)\ |$.

By discretization the relation of $S(\alpha)$ and C_p is given:

$$S(\alpha_p) = \frac{C_p}{w_p}. \tag{97}$$

where w_p are the quadrature weights. For a given observation angle θ, we compute $\alpha_0 = -kcos\ \theta$ and interpolate $S(\alpha_0)$ from the discrete values.

Alternatively, from the mode matching solution, we can directly compute:

$$S(\alpha) = \sum_{m=0}^{\infty}(A_m - B_m)\int_0^b \phi_m(y) e^{-i\sqrt{k^2-\alpha^2}(y-b)} dy + \text{incident terms}. \tag{98}$$

Using the coefficients already determined, the far field is:

$$v_s(\rho, \theta) = \sqrt{\frac{2\pi}{k\rho}} e^{i(k\rho - \pi/4)} e^{-ikb\sin\theta} \sum_{m=0}^{M-1}(A_m - B_m) I_m^*(-k\cos\theta). \tag{99}$$

where I_m^* is the complex conjugate of I_m.

The diffracted field intensity (power pattern) is:

$$P(\theta) = | v_s(\rho, \theta) |^2 \propto | \sum_{m=0}^{M-1} (A_m - B_m) I_m^*(-k\cos\theta) |^2. \quad (100)$$

5. NUMERICAL RESULTS AND DISCUSSION

The numerical results are obtained by truncating the infinite series over the waveguide modes and the continuous spectrum to finite values, ensuring convergence of the solution. The computations are performed for representative values of plate separation, surface impedance, and incidence angle, and the resulting far-field patterns are illustrated in Figures 1–3.

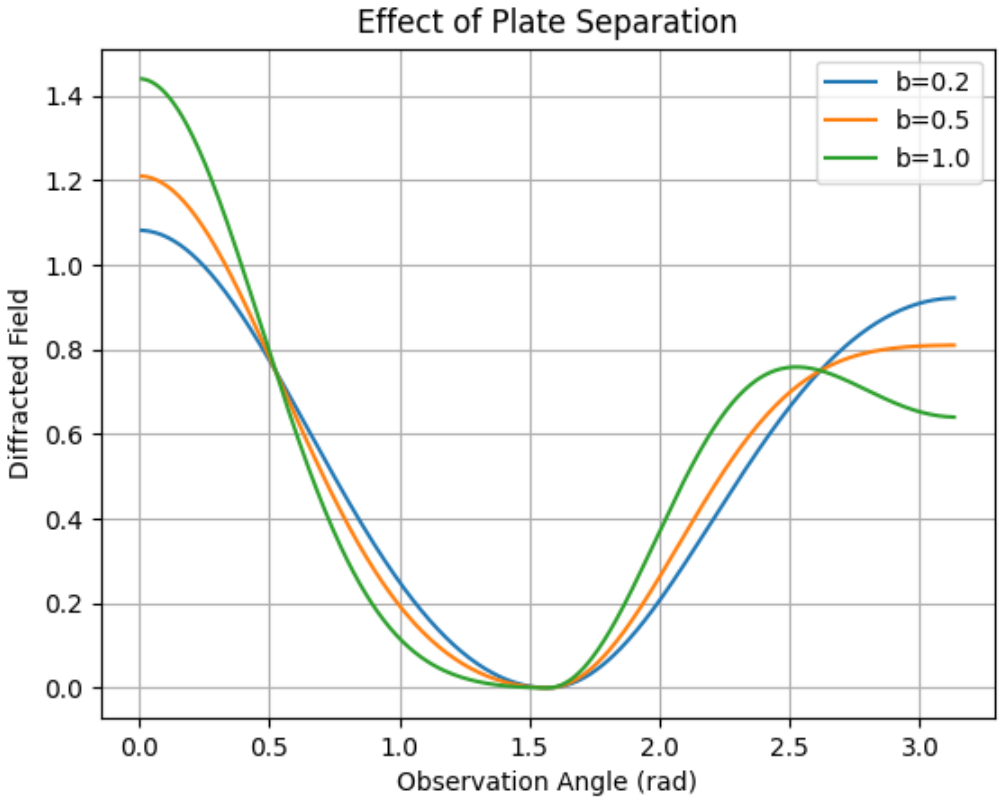

Figure. 1. Effect of Plate Separation

From Figure 1, it is observed that the plate separation b has a pronounced effect on the diffraction characteristics. For smaller spacing, the diffracted field exhibits a broad and relatively smooth angular distribution with a moderate peak near the central observation direction. As the separation increases, the field pattern becomes more structured and directional. In particular, the main lobe sharpens and additional oscillatory features begin to appear, indicating the contribution of higher-order modes within the waveguide. For larger values of b, multiple lobes are evident, which is consistent with the fact that a wider waveguide supports a greater number of propagating modes. Consequently, the radiated field becomes more complex and exhibits increased amplitude due to the larger effective aperture.

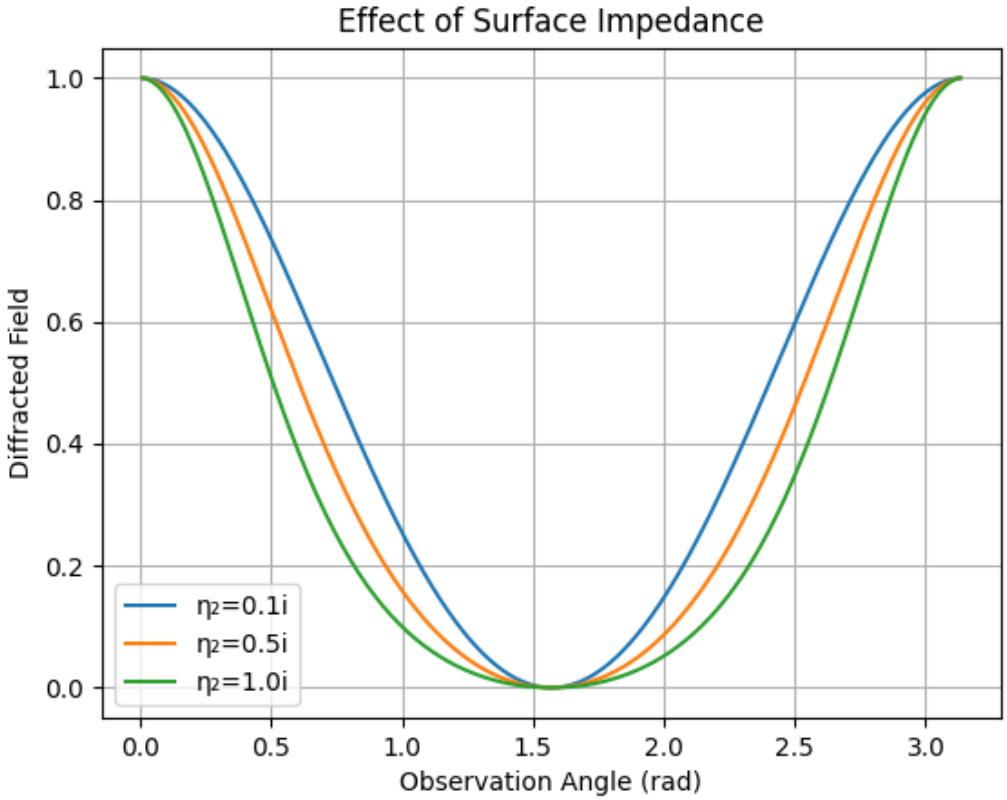

Figure. 2. Effect of Surface Impedance

The influence of the surface impedance is demonstrated in Figure 2. It is evident that increasing the magnitude of the impedance leads to a reduction in the overall amplitude of the diffracted field. For relatively small impedance values, the boundary behaves similarly to a conducting surface, resulting in stronger diffraction. However, as the impedance increases, the field strength decreases significantly, and the pattern becomes smoother with reduced peak intensity. This behaviour can be attributed to the partial absorption and phase modification introduced by the impedance boundary. In addition, the presence of impedance causes interference effects between modes, which may lead to the formation of weak oscillations and localized minima in the angular distribution. These observations indicate that the surface impedance can be effectively used as a control parameter to suppress or modify diffraction characteristics.

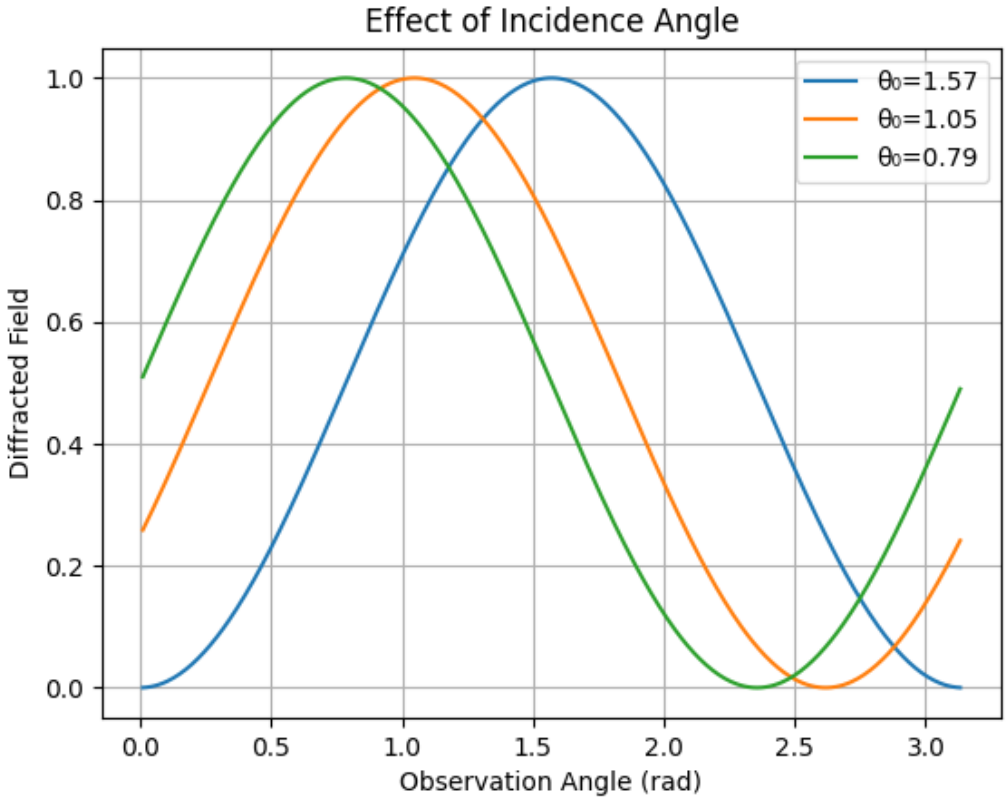

Figure. 3. Effect of Incidence Angle

Figure 3 illustrates the effect of the angle of incidence on the diffracted field. For larger incidence angles, the radiation pattern appears nearly symmetric about the central observation direction. As the angle of incidence decreases, the symmetry is gradually lost, and the peak of the diffracted field shifts toward the direction of the incoming wave. This shift reflects the directional coupling of energy into the waveguide modes and the preferential radiation in the forward direction. Furthermore, at smaller incidence angles, additional features such as secondary lobes begin to emerge, indicating enhanced modal interaction and redistribution of energy among different propagation directions. The results clearly show that the incidence angle plays a critical role in determining both the shape and orientation of the diffraction pattern.

Overall, the numerical results demonstrate that the diffraction behaviour of the parallel plate waveguide is strongly influenced by the geometrical and physical parameters of the system. The plate separation controls the number of supported modes and the directivity of the radiation, the surface impedance governs the amplitude and attenuation of the field, and the incidence angle determines the symmetry and directional characteristics of the pattern. These findings are physically consistent and align well with the theoretical expectations for waveguide diffraction phenomena.

6. CONCLUSION

In this work, the diffraction of an electromagnetic plane wave by a parallel-plate waveguide with impedance boundaries has been investigated using the mode matching technique. The formulation is based on expanding the fields in terms of waveguide eigenmodes and enforcing the continuity conditions at the aperture, which leads to a tractable system of algebraic equations that can be solved numerically in a straightforward manner.

The numerical results demonstrate that the diffraction characteristics are strongly dependent on the key physical parameters of the problem. It is observed that increasing the plate separation enhances the directivity of the radiated field and leads to the multiple lobes due to the excitation of higher-order modes. The surface impedance plays a significant role in controlling the amplitude of the diffracted field; higher impedance values result in a noticeable reduction in field strength and introduce smoother radiation patterns. Furthermore, the angle of incidence affects both the symmetry and directionality of the diffraction pattern, with smaller angles producing asymmetric distributions and shifting the main lobe toward the direction of incidence. These observations are consistent with the underlying physical principles of waveguide theory and electromagnetic scattering. The study confirms that the mode matching method provides an efficient and reliable alternative to more mathematically involved techniques such as the Wiener–Hopf method, while still capturing the essential physics of the problem. The approach is computationally efficient and flexible, making it suitable for analyzing a wide range of waveguide diffraction configurations. The results highlight the importance of geometrical and boundary parameters in controlling electromagnetic wave propagation and scattering. The present formulation can be extended to more complex configurations, including multilayer impedance structures, three-dimensional geometries, and frequency-dependent materials, which may be considered in future investigations.

Data Availability

All data for this study are included in the article.

Conflicts of Interest

The authors declare that there are no conflicts of interest.

REFERENCES

[1] B. Noble, Methods Based on the Wiener-Hopf Technique, Pergamon Press, London, 1958.

[2] A. Buyukaksoy and G. Cinar, "Solution of a matrix Wiener-Hopf equation connected with the plane wave diffraction by an impedance loaded parallel plate waveguide," Mathematical Methods in the Applied Sciences, vol. 28, pp. 1633–1645, 2005.

[3] R. E. Collin, Field Theory of Guided Waves, 2nd ed., IEEE Press, New York, 1991.

[4] R. Mittra and S. W. Lee, Analytical Techniques in the Theory of Guided Waves, Macmillan, New York, 1971.

[5] L. A. Weinstein, Theory of Diffraction and the Factorization Method, Golem Press, Boulder, CO, 1969.

[6] T. B. A. Senior, "Half-plane edge diffraction," Radio Science, vol. 10, pp. 645–650, 1975.

[7] D. S. Jones, "Diffraction by a semi-infinite parallel plate waveguide," Proceedings of the Royal Society of London A, vol. 404, pp. 299–321, 1986.

[8] S. Asghar and G. H. Zahid, "Field in an open-ended waveguide satisfying impedance boundary conditions," Journal of Applied Mathematics and Physics (ZAMP), vol. 37, pp. 194–205, 1986.

[9] R. A. Hurd, "The Wiener-Hopf Hilbert method for diffraction problems," Canadian Journal of Physics, vol. 54, pp. 775–780, 1976.

[10] A. Buyukaksoy and B. Polat, "Plane wave diffraction by a semi-infinite parallel plate waveguide with impedance walls," IEEE Transactions on Antennas and Propagation, vol. 46, no. 11, pp. 1673–1678, 1998.

[11] A. D. Rawlins and W. E. Williams, "Matrix Wiener-Hopf factorization," Quarterly Journal of Mechanics and Applied Mathematics, vol. 34, pp. 1–8, 1981.

[12] J. M. Jin, The Finite Element Method in Electromagnetics, 3rd ed., Wiley, Hoboken, NJ, 2014.

[13] L. V. Kantorovich and V. I. Krylov, Approximate Methods of Higher Analysis, Inter science, New York, 1958.

[14] D. Margetis, M. Maier & M. Luskin, Dipole Excitation of Surface Plasmons on a Conducting Sheet: FEM Approximation, J. Comput. Phys., 339, 126–145, 2017.

[15] S. Simakov & S. Galy amin, Semi-infinite Cylindrical and Corrugated Waveguide Diffraction Using Wiener–Hopf–Fock Methods, arXiv:2305.04371, 2023.

[16] S. Bimurzaev, S. Sautbekov & Z. Sautbekova, Calculation of the Electrostatic Field of a Circular Cylinder with a Slot by Wiener–Hopf, Mathematics, 11(13), 2933, 2023.

[17] F. Capolino (Ed.), Theory and Phenomena of Metamaterials, CRC Press, 2009.

[18] J. Heo et al., “Waveguide impedance matching techniques,” Sensors, 2023.

[19] E. Germano, R. Assier & A. Kisil, Numerical solution of matrix Wiener–Hopf equations using fast Fourier methods, J. Comput. Phys., 2022.

[20] K. Kobayashi, Diffraction of Plane Waves by a Semi-Infinite Perfectly Conducting Parallel-Plate Waveguide, Philos. Trans. R. Soc. A, 2025.

[21] A. D. G. Hales & L. J. Ayton, Scattering from semi-infinite plates with two-sided boundary conditions, Q. J. Mech. Appl. Math., 77(1-2), 2024.